Pergamon

Journal of Structural Geology, Vol. 16, No. 3, pp. 393 to 401, 1994

0191-8141/94 $06.00 + 0.00

Dip analysis as a tool for estimating regional kinematics in extensional terranes

DEBORAH L. SCOTT, JEAN BRAUN and MICHAEL A. ETHERIDGE

Research School of Earth Sciences, Australian National University, Canberra, ACT 0200, Australia

(*Received* 17 *July* 1992; *accepted in revised form* 25 *May* 1993)

Abstract—In basin analyses that rely almost solely on seismic reflection data to configure the underlying structure, it has become common practice to use extensional fault geometries to infer kinematic histories. This procedure relies on the existence of fault geometries predicted by ideal orthogonal extension and assumes the structure is well constrained. In areas where data are sparse or of equivocal quality this often leads to circular analysis. That is, ideal orthogonal extension is assumed to have been operative, then under-constrained fault geometries are mapped according to model predictions. Fault geometries so derived are subsequently used as evidence that orthogonal extension was operative and that the direction of extension is determinable. We develop an alternative tool for inferring kinematics which is independent of fault geometries. The method relies on the empirical evidence that the dip of the hangingwall(s) is systematic and predictable in extensional systems, even when fault geometries are non-ideal. Although not without significant limitations, dip analysis can provide additional constraints for structural and kinematic interpretations, especially where seismic reflection data are the main source of information and dip domains define discrete crustal blocks.

INTRODUCTION

IN RECENT years a plethora of seismic reflection data have become available to analyse basins, especially submerged basins where hydrocarbon prospectivity is high. These data are often the only source of information for the interpretation of structures that formed the basin. Fault geometries thus derived are frequently ambiguous, but are nonetheless used to infer regional tectonic kinematics, particularly in extensional terrains. Ideal orthogonal extension and/or strike-slip deformation models predict a simple relationship between the primary fault geometries and regional kinematics. Geometric models which imply different kinematic histories range between:

(1) orthogonal extension in which extension perpendicular to a rift axis or elongation gives rise to normal faults that strike parallel to and transfer faults that strike perpendicular to the rift axis (e.g. Lister *et al.* 1986); and

(2) strike-slip motion producing pull-apart basins, or rhombochasms, wherein the strike-slip faults are parallel to the rift elongation and normal faults range from 60° to 120° to the rift axis (e.g. Aydin & Nur 1982, Mann *et al.* 1983, Sylvester 1988).

Each model predicts a simple relationship between the rift or basin elongation, the geometry of the principal fault sets and the regional kinematics or tectonic transport direction. However, in the absence of geological kinematic indicators, estimating tectonic kinematics from fault geometries is only as valid as the structural interpretation is constrained.

It is common practice when evaluating a basin for resources to produce depth-to-horizon structure contour maps. These maps are, in essence, a picture of the dip of the surface of interest. Apparent dip directions as measured perpendicular to contours on the surface may not reflect the actual dip direction as measured at a point of control because to contour is to smooth. We effectively eliminate the information about the direction of the dip at our control points, which are located at profile intersections where two apparent dips are measurable, by contour shapes that are greatly influenced by the interpreters perceptions of fault geometries at the considered level. We present a method of inferring tectonic kinematics based on the dip of a surface using only the control points and therefore independent of interpretative contouring or fault geometries. The rotation or tilting of infra-basinal basement blocks determined at intersections of seismic profiles is used to establish a tectonic transport direction. We refer to this type of analysis as dip analysis. Dip analysis can be performed independently from *a priori* knowledge of fault geometries, thus providing corroborative evidence for interpreted fault patterns. Further, empirical evidence (Scott *et al.* 1992) suggests that the method can be used in areas where deformation is characterized by oblique-slip faults, even when extension-accommodating fault shapes and orientations vary throughout the system. Properly scaled analog sandbox modelling of extension accommodated by three-dimensional listric fault surfaces also supports this use of the dip of the hangingwall in non-ideal extension (Braun *et al.* in press).

Reflection seismic data are generally collected in a grid pattern providing the necessary large number of data points required to use dip analysis effectively. Dip analysis is particularly suited to these data because profile intersections provide two apparent dips of the block underlying the line(s) tie. The apparent dips can be used to determine the direction of the true (maximum) dip of the upper surface of the rotated or tilted block. If accurate velocity data are available, depth converted sections are preferred. However, the velocity

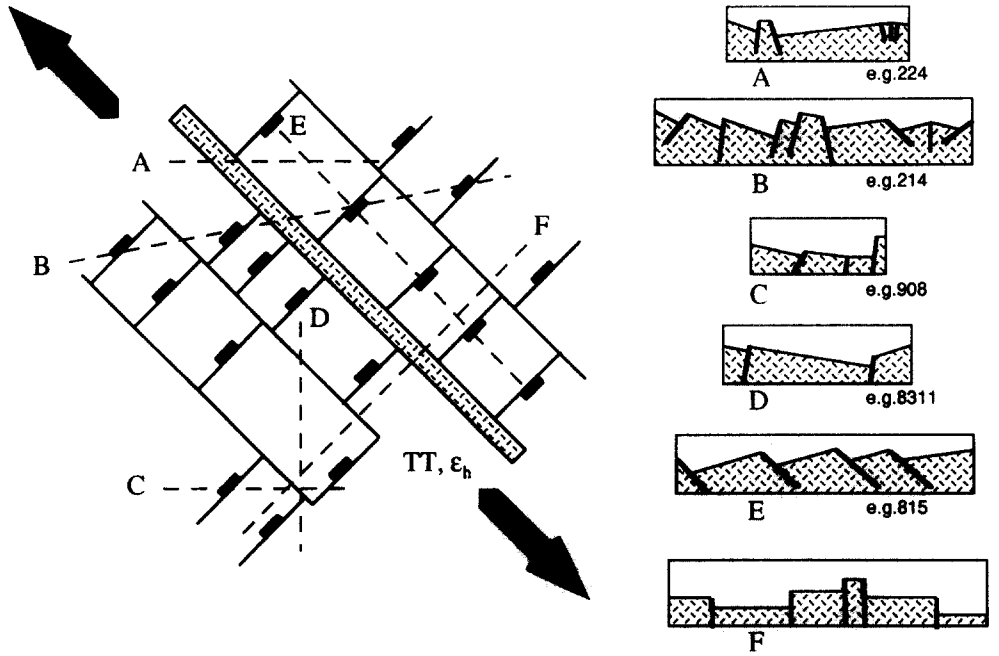

Fig. 1. Relationship of various profile geometries to an idealized extensional system. Heavy arrows indicate direction of regional extension, ε_h and tectonic transport direction, TT. Solid lines parallel to ε_h are sub-vertical transfer faults which decouple adjacent half-grabens by oblique- to strike-slip motion. Solid lines perpendicular to ε_h and marked by heavy tick marks are normal (dip-slip) faults. Profiles A–F show predicted basement geometries of variously oriented seismic profiles. Only geometries E and F aligned parallel and perpendicular to ε_h are reconstructible in the plane of the profile at basement levels. Profile geometries are derived from East African Rift data, numbers refer to line numbers as published in Rosendahl *et al.* (1986, 1988), Rosendahl (1987) and Scholz *et al.* (1989).

profile at the point of intersection is identical on both profiles and reflections will be moved identically on each depth converted section. If lateral facies changes away from that point in the direction of each of the profiles are radically different the *direction* of the true dip computed from time or depth sections will be different. However, in most cases we have encountered the direction of the dip remains consistent in both data forms (e.g. Stone 1991, Hoffman & Reston 1992). Likewise, the direction remains largely unaffected by the migration process, although the magnitude of the dip will vary in each of these processed data forms. Because reflection seismic data are normally acquired in a grid, intersections tend to be abundant, thus providing a sufficient database to provide statistical credence to the dip direction determination. However, regional dips in the pre-deformation setting and depositional dips may yield an apparent consistency which is not due to tectonic processes. As with all observational methods, care in discerning the possibilities for error is advised.

In the following sections, we outline geometric concepts relating fault geometries to tectonic kinematics in ideal model terms. The relationships between fault geometries imaged in seismic profiles, block rotations or tilting and direction of tectonic transport on the system scale are considered. We evaluate individual block rotations and the significance of the dip of the block to develop dip analysis. We demonstrate the validity of the method in the ideal orthogonal extension case. To explain observational data, the geometric relationships in the ideal, orthogonal deformation scenario are hypothetically extrapolated to situations where extension is non-ideal and accommodated by oblique-slip faults, and some possible rationales are explored. Finally, we apply the method to some reflection seismic data to demonstrate the strengths and limitations of dip interpretation in basin analysis.

EXTENSIONAL (RIFT) SYSTEMS

Currently accepted models of ideal orthogonal extension in the upper brittle crust predict two distinct fault sets which are mutually perpendicular and lead to simple fault–basement-dip geometries in cross-sections aligned perpendicular to the fault sets (profiles E and F, Fig. 1). These ideal models suggest that rift elongation is most commonly perpendicular to the direction of horizontal extension, ε_h, mimicking geometries at oceanic spreading centres. 'Dip lines' parallel to ε_h or the tectonic transport direction will show a series of similarly tilted fault blocks bounded by normal faults (e.g. profile E, Fig. 1). Deformation is balanceable or retrodeformable (Suppe 1985) in the plane of the profile. 'Strike lines' parallel to the traces of normal faults will image flat-lying subsided blocks and vertical faults (e.g. profile F, Fig. 1). 'Strike line' geometry may appear reconstructible at the basement surface by purely vertical motion along the faults, but this is not a correct reversal of movement on these fault planes, and normally the overlying syn-rift beds will not retrodeform by this motion. Profiles in *any other orientation* will image unbalanceable geometries in the profile plane (e.g. profiles A–D, Fig. 1). That is, gaps or overlaps appear when

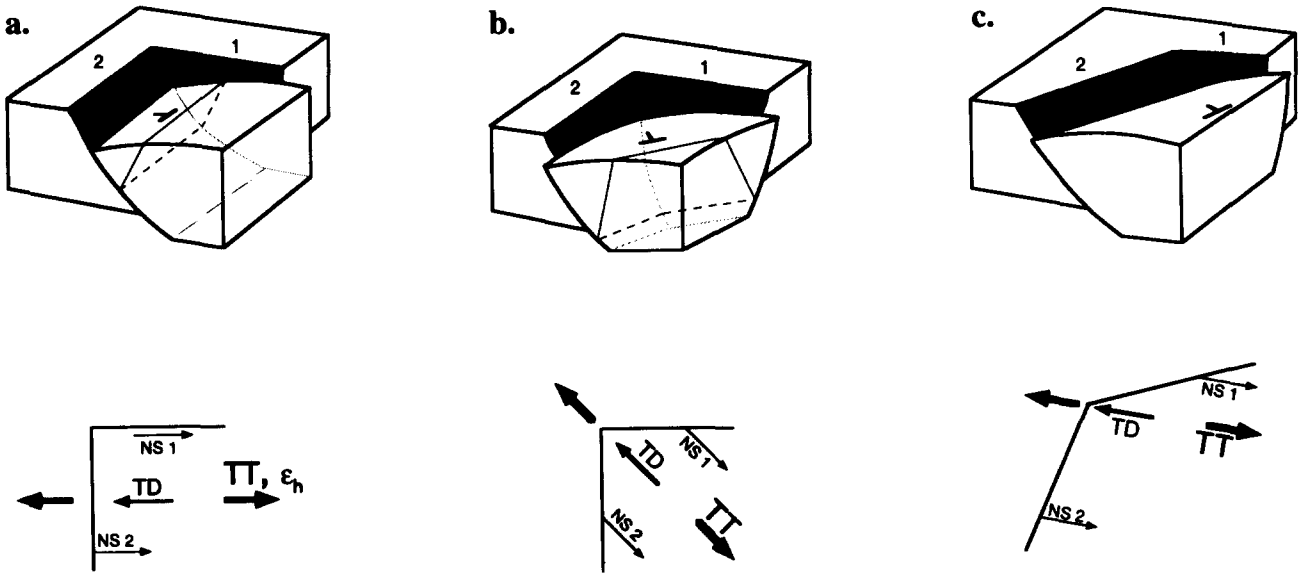

Fig. 2. Block diagrams and plan views illustrating the relationship between fault geometries, hangingwall dip direction and tectonic transport direction. Heavy arrows labelled TT = direction of tectonic transport, mid-weight arrow labelled TD = direction of true dip of tilted–rotated block, light-weight arrows labelled NS1 or 2 = net slip vector of faults with corresponding numbers in block diagram projected to the horizontal. Block diagrams are drawn with straight faults with no detachment for clarity. The same principles apply to listric faults that sole at depth as demonstrated in Fig. 3 and Appendix 1. (a) Orthogonal–rectilinear deformation with a normal (dip-slip) fault perpendicular to and a transfer (oblique- to strike-slip) fault parallel to the direction of extension (TT). (b) Orthogonal faults each 45° from TT and with equal dips and curvature. (c) A common variation of fault orientations and dips. Fault 1 has minimal curvature and is misaligned with TT by no more than 30°. Fault 2 is sub-perpendicular to TT, but may be highly variable depending on the dip and orientation of fault 1 and basement fabric. Possible orientations of inclined shear planes that would produce the depicted dips of the hangingwall blocks are indicated in (a) and (b).

blocks are moved back along faults and movement in or out of the profile plane is not allowed. The 'dip line' orientation will image the fault(s) at its steepest and the *true dip* of the hangingwall block. Profiles at any other angle will image seemingly shallower fault and hangingwall dips. A profile oriented obliquely to a transfer fault may image an over-rotated hangingwall block compared to the steepness of the transfer fault or the hangingwall block may even dip away from apparent vertical offset on the transfer fault.

Movement on individual listric or planar extensional faults within rift systems invariably gives rise to rotation or tilting of adjacent fault blocks overlain by syn-rift sediments. The rotation, tilt or dip of the subsided blocks is measurable at seismic profile intersections. As is true of the profiles discussed above, the direction of the dips of an individual block within an orthogonally extending system is systematically related to the bounding fault geometry, the tectonic transport direction (TT) and ε_h (Fig. 2a). That is, *hangingwall dip direction is exactly opposite to the dip of the bounding fault if movement on the fault is pure dip-slip*. If a fault surface is non-planar or non-circular some internal deformation of the hangingwall will occur. When substantial non-elastic strain within the hangingwall modifies the block's geometry, dips of the hangingwall surface will vary depending on the mechanism of deformation. It is not within the scope of this study to detail the variations of dip caused by internal deformation and in the following discussion we assume no volume change or distortion of fault blocks. Despite the simplifying assumptions, empirical evidence from several rift settings (e.g. Scott *et al.* 1992, Marshall *et al.* 1993, Wise in press) suggests that dip analysis using a large database on a regional scale can enhance structural and kinematic interpretations.

Consider a single normal fault which accommodates extension perpendicular to it (fault 2 in Fig. 2a). The magnitude of the dip of the hangingwall block is determined by the curvature of the normal fault, the amount of displacement on it and any rotation of the fault due to movements on other faults in its footwall. However, the *direction* of the dip of the hangingwall block is perpendicular to the strike of the fault and is unaffected by the aforementioned parameters. A depth converted seismic line shot exactly perpendicular to the fault will image a recoverable or balanceable geometry. In this geometry, the dip direction of the hangingwall block is parallel to the transfer fault (1) and perpendicular to the normal fault (2). In plan view, the true dip direction (TD) of the hangingwall block is parallel but opposite to the trends of the net slip vectors of the transfer fault (NS1) and normal fault (NS2). The azimuth of NS and TD is the horizontal motion or tectonic transport (TT) direction of the subsided or rotated bock and is equivalent to ε_h. In the same system, a fault of the opposite polarity will have mirror image hangingwall dip, net slip and tectonic transport directions. The azimuth of NS, TD and TT is parallel to the trace of the intersection of the fault planes, which in this case is the direction of the transfer faults. Analytical and experimental models support these relationships for the case of orthogonal extension (Withjack & Jamison 1986).

When extension is accommodated by movement on non-ideally aligned fault surfaces, producing oblique-slip deformation, the relationship between fault geometry, the direction of maximum extension and the tectonic transport direction observed in orthogonal extension is less predictable. Indeed, depending on fault orientation it is arguable which faults are acting as transfer faults and which are the extension-accommodating normal faults. Likewise, the dips of the hangingwall are not as simply related to the fault geometry. For instance, in some primarily strike-slip terranes the hangingwall dip of oblique pull-apart basins is directly into the normal fault, regardless of the trend of the strike-slip fault sets, which correspond to slip or tectonic transport direction (Walker & Wernicke 1986). In contrast, strike-slip segments of the extensional East African Rift System (EARS) (e.g. the Rukwa rift, Scott *et al.* in press) have dips that are consistent with the extensional segments (e.g. the Tanganyika and Malawi rifts, Scott *et al.* 1992). Two oblique-slip geometries are presented in Figs. 2(b) & (c). The first oblique geometry mimics analog and analytical models that produce a large proportion of hangingwall dips parallel to the direction of extension rather than directly opposite the dips of non-ideally aligned fault surfaces (Braun *et al.* in press); the second geometry describes a slight deviation from the orthogonal case which we propose is a common geometry in rifted terranes.

Figure 2(b) shows mutually perpendicular faults that both strike at 45° to the direction of extension. The fault dips and curvature are also equal. The faults will have equal amounts of dip-slip, as well as equal components of strike-slip. As in the orthogonal fault geometry case, the trends of the net slip vectors (NS1 and NS2) of two linked oblique-slip faults, responding to the same extension, are parallel to each other and to the trace of the intersection of the two fault surfaces. The trend of the net slip vectors still gives the tectonic transport direction or displacement vector of the block as in the ideal orthogonal extension case (Fig. 2a).

An entire spectrum of fault set trends may theoretically exist, ranging from the ideal orthogonal to symmetrically oblique end-members discussed above. The possible geometries are limited only by the ability for movement to occur on a non-ideally aligned fault surface. Scotti *et al.* (1991) have provided convincing theoretical arguments that a fault surface may be rotated up to 75° from ideal alignment and still experience motion. The variation of the oblique-slip block geometry presented in Fig. 2(c) was originally derived from recent interpretations of EARS basins (Scott *et al.* 1992) and recurs in several rifted basins on Australian and South American passive margins that we have analysed using proprietary industry data.

In this geometry (Fig. 2c), fault 1 is substantially steeper than fault 2. Also, fault 1 is at a low angle and fault 2 is at a higher angle to the direction of extension. In other words, fault geometries deviate only slightly from the rectilinear patterns predicted by the orthogonal extension model. This geometry results in a higher component of dip-slip motion on fault 2 and a higher component of strike-slip motion on fault 1, yet the trends of the net slip vectors remain parallel to each other. The net slip vectors of both fault surfaces are parallel to the trace of the line of intersection of the fault surfaces which, as outlined below, describes the tectonic transport direction of the block. In the EARS, the consistency of the dip measurements suggests that the tectonic transport direction is equivalent in all of the structural domains regardless of their bounding fault orientation and whether or not extension is aligned perpendicular to rift elongation or to the main bounding faults. Below we outline a possible rationale for this relationship, even when the extensional fault surfaces are not perpendicular to the direction of extension and investigate the relationship between fault geometry and the hangingwall dip direction.

The relationship of the dip of the upper surface of the hangingwall block to the direction of tectonic transport in the oblique-slip cases (e.g. Figs. 2b & c) depends upon the shape of the fault surfaces and the mechanism of internal deformation of the block. Extensional deformation often leads to the formation of low-angle, listric normal faults which sole out into a detachment (e.g. Gibbs 1984, Lister *et al.* 1986, 1991, Etheridge *et al.* 1989, Dula 1991, Roberts *et al.* 1991, Forsyth 1992). If both fault surfaces have constant curvature, it can be shown that the intersection of the two fault surfaces lies in a vertical plane and the strike of this plane is the direction of motion or relative displacement (tectonic transport direction) of the hangingwall block (Appendix 1). The relationship of the co-ordinates of a random point on the intersection of two listric fault surfaces is:

$$x(\lambda_1 \sin \alpha_2 + \lambda_2 \sin \alpha_1) = y(\lambda_1 \cos \alpha_2 + \lambda_2 \cos \alpha_1), \quad (1)$$

where α_1 is the angle the strike of the fault, F_i, makes with the x-axis and λ_i characterizes the curvature of a fault as depicted in Fig. 3. If it is assumed that contact is maintained across the fault surfaces, motion of the hangingwall block is constrained to follow the 'track' defined by the intersection of the two planes (Appendix 1). The relationship in equation (1) is clearly linear and establishes the kinematic path of the block and the direction of maximum horizontal extension. This relationship holds true for any combination of curvatures for the two faults, regardless of their orientation with respect to each other. It applies particularly to local 'corners' made by two linked faults and where rotation or tilting of adjacent blocks into the faults occurs. However, if one fault is planar and not orthogonal to the other fault, the trace of the track is curvilinear. If the ratio of the curvatures changes, for example ramp and flat morphologies within a non-orthogonal extensional system, the intersection of the fault surfaces is not linear. In these cases local changes in dip direction may provide clues to fault geometries at depth.

If the fault surface curvature is characterized by anything other than a most unlikely circular function, the hangingwall must undergo some internal deformation in order to maintain contact across the fault plane. How

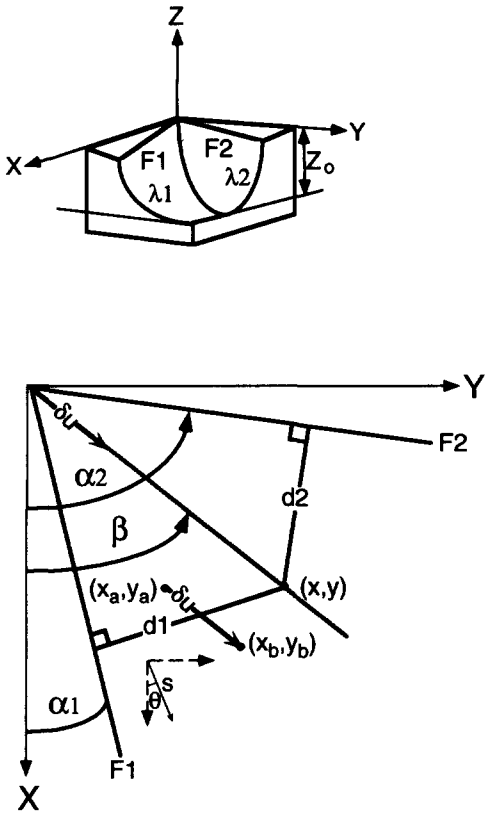

Fig. 3. Idealized three-dimensional portrayal of the 'corner' of two listric fault surfaces (F1 and F2) and a plan view labelled with the various angular and distance relationships of the faults. Z_0 is the depth to detachment. λs are constants characterizing the curvature of the fault surfaces. αs are the angle of the fault traces with the X-axis. ds are the perpendicular distance from the fault traces to the horizontal projection of an arbitrary point (x, y) on a fault surface. β is the computed angle of the horizontal trace of the intersection of the two fault surfaces with the X-axis. See Appendix 1 for a development of the relationships between variables.

the dip of the upper surface relates to the tectonic 'track' depends upon the internal deformation of the block, even in the simplest linear tectonic track case described in Fig. 3. Different deformation mechanisms produce different hangingwall block surface morphologies. However, it is still possible to use dip analysis to infer regional kinematics in most geologically reasonable situations. For example, consider the simple case of vertical shear developed for the general three-dimensional case in Appendix 2. Particles in the hangingwall block are constrained to subside in vertical columns to fill the gap caused by the displacement of the hangingwall away from the fault surfaces. In this case, dip directions on the top of the hangingwall will trend perpendicular to each of the bounding faults on either side of the tectonic track. Dip domains defined by fault compartments would be subdivided by a ridge aligned with and on top of the tectonic track. The morphology of the ridge yields information of the relative curvatures of the fault surfaces and their strikes. For example, if it bisects the two fault traces, a linked pair as shown in Fig. 2(b) may be inferred.

Various two-dimensional geometric models of roll-over (or dip of the upper hangingwall surface in orthogonal extension) and fault surfaces which consider a variety of internal deformation mechanisms have been investigated (e.g. Walker & Wernicke 1986, White *et al.* 1986, Williams & Vann 1987, Jackson *et al.* 1988, Groshong 1989, Walsh *et al.* 1991, Westaway 1992). The various internal deformation mechanisms alter the depth to detachment and magnitude of dip of the upper surface of the hangingwall slightly, but do not affect the dip *direction*, which is still aligned with the tectonic transport direction. However, Dula (1991) concludes that "the inclined shear (planar slip surfaces) and the related constant-displacement (curved slip surfaces) mechanism was the most successful in predicting observed clay-model and earth examples revealed in seismic data".

In the two-dimensional case, inclined shear planes trend parallel to the normal faults or perpendicular to the tectonic transport direction (Fig. 2a). If we invoke vertical or inclined shear planes aligned perpendicular to the tectonic transport direction in the three-dimensional geometry described by Figs. 2(b) and 3, the dip of the upper surface of the hangingwall block would align perpendicular to the shear planes or parallel to the tectonic transport direction. In other words, the shear plane or 'sheet' adjacent to the intersection of the two fault surfaces (i.e. the corner) would subside the most, with each successive 'sheet' subsiding less away from the 'corner' made by the adjoining faults. Modifications to this direction within each 'sheet' might be caused by increased subsidence adjacent to the faults as in the vertical shear column case discussed above. The effect of such a modification would depend primarily on the degree of curvature of the 'transfer' fault of the bounding fault pair and what angle the fault pair makes. It is obvious that as the angle of the faults deviate from rectilinear the system passes into the realm of strike-slip deformation.

Observational data from the EARS (Scott *et al.* 1992) suggest that the deviation of the 'transfer' fault from the direction of tectonic transport does not exceed 30° and is more commonly less than 15°. In contrast, the 'normal' faults vary widely from one dip domain to the next. The inclined-shear oriented perpendicular to tectonic transport internal deformation may explain the consistency of the dips measured in the EARS, given that major extensional fault trends appear to vary substantially along the rift. Alternatively, the deformation and subsequent hangingwall dips recorded in analog models of oblique-slip geometries is reproduced precisely by a recently developed analytical kinematic model requiring lines within the hangingwall block that are normal to the fault surface to remain normal after deformation (Braun *et al.* in press). To date, observational dip data from natural rift systems do not provide any reason to prefer either inclined shear or 'rule of the normal' internal deformation, although it strongly supports one or the other over dips predicted by vertical shear deformation as described above and in Appendix 2.

APPLICATION OF DIP ANALYSIS

The apparent dips of any two intersecting profiles over a rotated block are measurable and can be used to compute the direction of the true dip of the block. The measured direction of dips of 170 intra-rift blocks in the Lakes Malawi (Fig. 4) and Tanganyika rift zones of the EARS are remarkably consistent (Scott *et al.* 1992). They are consistent along more than 1000 km of the rift even though they are derived from a variety of structural domains, defined by composite half grabens with bounding faults of varying trends (Rosendahl 1987). The profiles shown in Fig. 5 are intersecting profiles from the N–S-trending Lake Malawi rift zone (Fig. 4) of the EARS.

The data and interpretations presented in Fig. 5 are taken from Scholz *et al.* (1989) and demonstrate the use of dip analysis as well as some of its limitations. The segment of Line 815 (top panels) images a series of synthetic tilted fault blocks whose whole profile geometry is that of a 'classic' dip line. The bold arrow locates where the left tilt block is intersected by Line 938 (bottom panels). This portion of Line 938 has been interpreted to be a single westward tilting block, cut by two minor intra-block antithetic faults. The overall apparent dip of the basement is to the west on both profiles, suggesting correlation of the faults labelled F and a true dip in the direction that bisects the trend of the profiles, or about 280°. Note, however, that the base syn-rift reflection at the profile tie in the uninterpreted section of Line 938 is practically flat-lying. Further, the reflection retains this dip until a disruption of the reflection to the left (Fig. 5, 'D'), where its dip steepens before reaching the interpreted bounding fault. Also, the rotation in the footwall of fault F is quite different in each profile. Using the measurements displayed in Fig. 5, the dip of the block underlying the profile intersection trends 318°. Dips determined for adjacent blocks along this profile, determined at the intersections of this profile with other NE-trending profiles are within 1° of the 318° trend. This direction is in agreement with the regionally determined tectonic transport direction (Scott *et al.* 1992). We suggest that the 'classic dip geometry' suggested by Line 815 (Fig. 1, profile E) is due to the profiles near perfect alignment with the direction of tectonic transport, even though it is oblique to the rift axis. These data support a NW–SE direction of extension as determined by onshore fault slip data (Chorowicz & Sorlien 1992), rather than the E–W direction inferred from the rift elongation and earlier interpretations of fault geometries (Sander 1986, Morley *et al.* 1989, 1990).

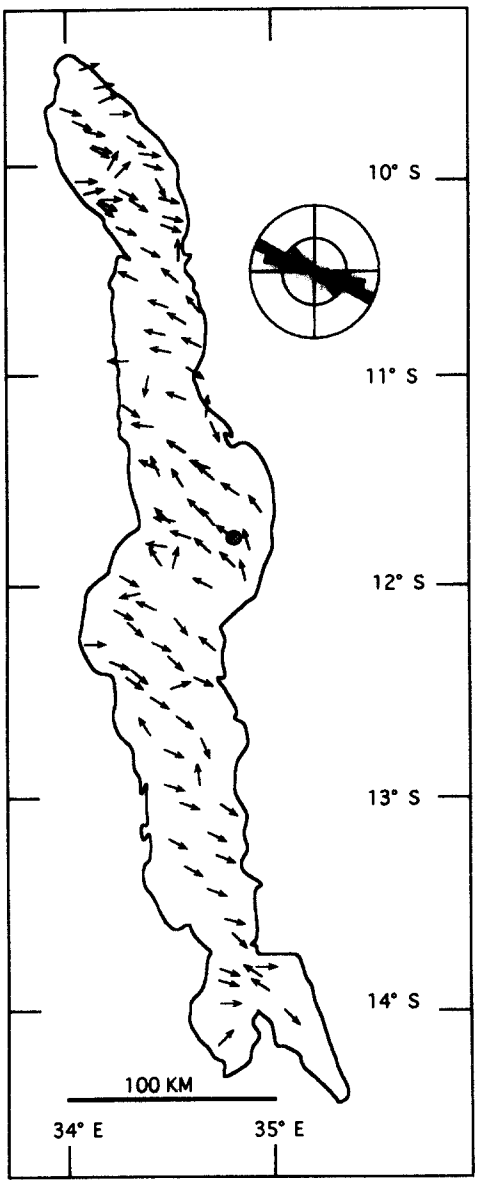

Fig. 4. Computed dip directions of blocks underlying seismic profile intersections in the Lake Malawi rift zone of the East African Rift. There are 108 control points plotted and used in the rose diagram. The rift zone is compartmentalized by dip domains which are internally consistent within 5–10°.

Dip analysis can also help the interpreter with individual fault correlations. Previous interpretations (Scholz *et al.* 1989) correlated faults F in Fig. 5, which produces a structure striking nearly N–S at about 015°. However, the computed dip of the block underlying the profile intersection suggests a normal fault striking perpendicular to the dip at 048°. Ideal orthogonal extension models would then predict transfer faults parallel to the dip direction. Perhaps the disruption of the reflection on Line 938 (Fig. 5, 'D') is a transfer structure that offsets an appropriately aligned (that is, perpendicular to the dip of the hangingwall) normal fault at F on both profiles. If there are unambiguous fault correlations which do not align in these directions, then an interpreter is signalled to develop an interpretation which incorporates pairs of faults which can produce this direction of dip or to consider interpretations with considerable internal deformation of the blocks.

It should be noted that a small error in the measurement of the apparent dips in the example in Fig. 5 can produce a significant change in the determined dip direction, emphasizing the need for a large dataset which yields a consistent result. Care must also be taken to account for anomalies in the seismic reflection method such as velocity anomalies near fault planes or

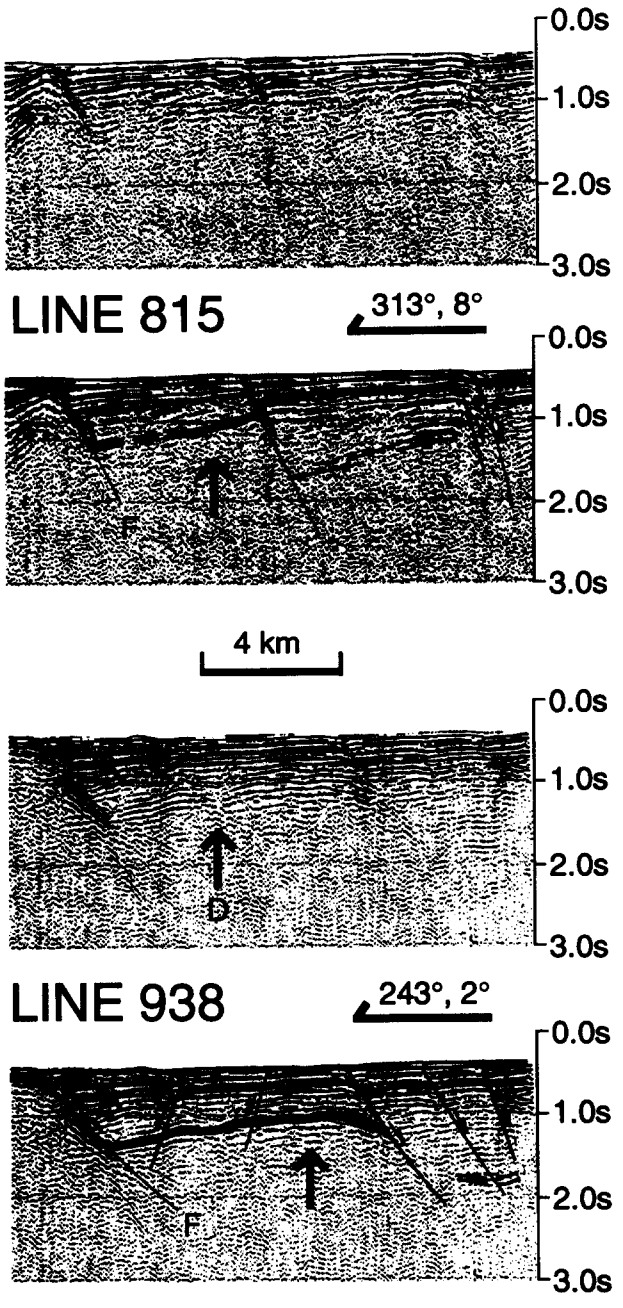

Fig. 5. Sections of unmigrated multifold seismic lines 815 and 938 from Lake Malawi, East Africa. Interpretations are from Scholz *et al.* (1989). Bold arrows indicate the location of the intersection of the two profiles. The strike of the profile and the apparent dip of acoustic basement at the point of intersection are indicated above each interpreted section. 'D' on the uninterpreted Line 938 profile indicates a disruption and change in apparent dip of the acoustic basement reflection as discussed in text.

lateral velocity changes in time sections. Distortions within the syn-rift package due to differential compaction, reverse drag or folding along normal faults must also be considered, especially where acoustic basement is not clearly pre-rift basement. Depositional dip or pre-extension regional dip may introduce systematic errors into the analysis. This type of analysis of rifted passive margins is limited by knowledge of post-rift deformation such as thermal subsidence or post-rift fault reactivation. However, if these factors are regionally consistent it may be possible to 'back strip' their effect with good result.

DISCUSSION AND CONCLUSIONS

As any reflection seismic data interpreter will attest, interpretation of these data is commonly ambiguous. Spacing of the acquisition grid often is the controlling factor in precision of the fault correlations. Subtleties such as the dip change in Line 938 (Fig. 5) are often missed. If the structure is complex or the seismic data are poor the problem is exacerbated. In most cases, dip of the acoustic basement and/or base of the syn-rift sequence is more easily determined than fault trends. Where dip analysis provides a consistent result with a sufficiently large dataset, it may be used to constrain tectonic kinematics, internal deformation mechanisms and fault geometries, as only a few combinations will produce this consistency. Locally, dip analysis can provide guidance for fault correlations between profiles where they are not well constrained by data. Where dips are locally inconsistent with the regional set, the interpreter is signalled to look for non-ideally aligned faults or changes in the fault surfaces at depth.

It is also apparent that, depending on the variance of the fault geometries from rectilinear, areas of polarity reversals (i.e. sense of asymmetry) or changes in adjacent half-graben bounding fault geometries will be areas of 'non-ideal' oblique-slip deformation and may have anomalous dips due to local wrenching or even compression. Finally, convincing kinematic interpretations derived from dip analysis rely heavily on having a large, areally extensive, statistically credible dataset.

We propose that in the absence of geological kinematic indicators, the dip method is a more robust tool for constraining regional kinematics than fault trends, and when combined with careful fault correlations it adds to the confidence of inferred kinematic histories. The method is particularly useful in extensional terrains where seismic reflection data are the primary source of information. Further, dip analysis allows for the identification of dip domains which must be separated by faults that decouple dissimilar basement dips, thereby identifying structures even where the faults are not directly imaged. Although there are various possible fault geometries in oblique-slip deformation models, in the simple cases considered here true dip direction of the hanging-wall block aligns with the tectonic transport direction and is a reliable kinematic indicator if sufficient measurements are available over a regionally consistent tectonic terrain, regardless of the strike or dip of the faults that bound the block(s).

Acknowledgements—The authors thank B. Rosendahl and the Department of Geology, Duke University for permission to access the PROBE seismic data from East Africa. D. Scott is indebted to T. Purcell for assistance in computer programs and acknowledges with appreciation many helpful discussions with G. Irwin. The manuscript was improved by a particularly constructive and conscientious review

by D. Shultz-Ela. Financial support for D. Scott from Marathon Petroleum (Australia) is gratefully acknowledged.

REFERENCES

Aydin, A. & Nur, A. 1982. Evolution of pull-apart basins and their scale independence. *Tectonics* **1**, 91–105.

Braun, J., Batt, G. E., Scott, D. L., McQueen, H. & Beasley, T. In press. A simple kinematic model for crustal deformation along two- and three-dimensional listric normal faults derived from scaled laboratory experiments. *J. Struct. Geol.*

Chorowicz, J. & Sorlien, C. 1992. Oblique extensional tectonics in the Malawi Rift, Africa. *Bull. geol. Soc. Am.* **104**, 1015–1023.

Dula, W. F., Jr. 1991. Geometric models of listric normal faults and rollover folds. *Bull. Am. Ass. Petrol. Geol.* **75**, 1609–1625.

Etheridge, M. A., Symonds, P. A. & Lister, G. S. 1989. Application of the detachment model to reconstruction of conjugate passive margins. *Mem. Am. Ass. Petrol. Geol.* **46**, 23–40.

Forsyth, D. W. 1992. Finite extension and low-angle normal faulting. *Geology* **20**, 20–27.

Gibbs, A. D. 1984. Structural evolution of extensional basin margins. *J. geol. Soc. Lond.* **141**, 609–620.

Groshong, R. H., Jr. 1989. Half-graben structures: balanced models of extensional fault-bend folds. *Bull. geol. Soc. Am.* **101**, 96–105.

Hoffman, H. J. & Reston, T. J. 1992. Nature of the S reflector beneath the Galicia Banks rifted margin: Preliminary results from prestack depth migration. *Geology* **20**, 1091–1094.

Jackson, J. A., White, N. J., Garfunkel, Z. & Anderson, H. 1988. Relations between normal-fault geometry, tilting and vertical motions in extensional terrains: an example from the southern Gulf of Suez. *J. Struct. Geol.* **10**, 155–170.

King, G. & Cisternas, A. 1991. Do little things matter? *Nature* **351**, 350.

Lister, G. S., Etheridge, M. A. & Symonds, P. A. 1986. Detachment faulting and the evolution of passive continental margins. *Geology* **14**, 245–250.

Lister, G. S., Etheridge, M. A. & Symonds, P. A. 1991. Detachment models for the formation of passive continental margins. *Tectonics* **10**, 1038–1064.

Mann, P., Hempton, M. R., Bradley, D. C. & Burke, K. 1983. Development of pull-apart basins. *J. Geol.* **91**, 529–554.

Marshall, J. F., Ramsay, D. C., Moore, A. M. G., Shafik, S., Graham, T. G. & Needham, J. 1993. The Vlaming Sub-basin: Offshore South Perth Basin. Continental Margins Program, Australian Geological Survey Organization, folio 7.

Morley, C. K., Nelson, R. A., Patton, T. L. & Munn, S. G. 1990. Transfer zones in the East African Rift System and their relevance to hydrocarbon exploration in rifts. *Bull. Am. Ass. Petrol. Geol.* **74**, 1234–1253.

Morley, C. K., Westcott, W. A., Cunningham, S. M. & Harper, R. M. 1989. Recent exploration in the Lake Rukwa area, East African Rift. *Proc. 28th Int. Geol. Congr.* (Washington, DC), 2-462–2-463.

Roberts, A. M., Yielding, G. & Freeman, B. (editors). 1991. *The Geometry of Normal Faults. Spec. Publs geol. Soc. Lond.* **56**.

Rosendahl, B. R. 1987. Architecture of continental rifts with special reference to East Africa. *Annu. Rev. Earth & Planet. Sci.* **15**, 445–503.

Rosendahl, B. R., Reynolds, D. J., Lorber, P. M., Burgess, C. F., McGill, J., Scott, D., Lambiase, J. J. & Derksen, S. J. 1986. Structural expressions of rifting: Lessons from Lake Tanganyika, Africa. In: *Sedimentation in the African Rifts* (edited by Frostick, L. E., Renaut, R. W., Reid, I. & Tiercelin, J. J.). *Spec. Publs geol. Soc. Lond.* **25**, 29–43.

Rosendahl, B. R., Versfelt, J. W., Scholz, C. A., Buck, J. E. & Woods, L. D. 1988. Seismic atlas of Lake Tanganyika, East Africa. *Project PROBE Geophys. Atlas Ser.* Duke University, Durham, folio 1.

Sander, S. 1986. The geometry of rifting in Lake Tanganyika, East Africa. Unpublished M.Sc. thesis, Duke University.

Scholz, C. A., Rosendahl, B. R., Versfelt, J. W., Kaczmarick, K. J. & Woods, L. D. 1989. Seismic atlas of Lake Malawi (Nyasa), East Africa. *Project PROBE Geophys. Atlas Ser.* Duke University, Durham, folio 2.

Scott, D. L., Etheridge, M. A. & Rosendahl, B. R. 1992. Oblique-slip deformation in extensional terrains: a case study from the Lakes Tanganyika and Malawi rift zones, East Africa. *Tectonics* **11**, 998–1009.

Scott, D. L., Kilembe, E. A. & Rosendahl, B. R. In press. Dip domain analysis of Lake Rukwa Rift, East Africa: An intra-continental transform? *Geology*.

Scotti, O., Nur, A. & Estevez, R. 1991. Distributed deformation and block rotation in three dimensions. *J. geophys. Res.* **96**, 12,225–12,243.

Stone, D. S. 1991. Analysis of scale exaggeration on seismic profiles. *Bull. Am. Ass. Petrol. Geol.* **75**, 1161–1177.

Suppe, J. 1985. *Principles of Structural Geology*. Prentice-Hall, Englewood Cliffs, New Jersey.

Sylvester, A. G. 1988. Strike-slip faults. *Bull. geol. Soc. Am.* **100**, 1666–1703.

Walker, J. D. & Wernicke, B. P. 1986. The relation of tilt geometry to extension direction. (Abs.) *Geol. Soc. Am. Abs. w. Prog.* **194**.

Walsh, J., Watterson, J. & Yielding, G. 1991. The importance of small-scale faulting in regional extension. *Nature* **351**, 391–393.

Westaway, R. 1992. Analysis of tilting near normal faults using calculus of variations: implications for upper crustal stress and rheology. *J. Struct. Geol.* **14**, 857–871.

White, N. J., Jackson, J. A. & McKenzie, D. P. 1986. The relationship between the geometry of normal faults and that of the sedimentary layers in their hanging walls. *J. Struct. Geol.* **8**, 897–909.

Williams, G. & Vann, I. 1987. The geometry of listric normal faults and deformation in their hangingwall. *J. Struct. Geol.* **9**, 789–795.

Wise, D. U. In press. Dip domain method applied to the mesozoic Connecticut Valley rift basins. *Tectonics*.

Withjack, M. O. & Jamison, W. R. 1986. Deformation produced by oblique rifting. *Tectonophysics* **126**, 99–124.

APPENDIX 1

Derivation of the 'tectonic track' in a three-dimensional listric fault system

Consider the two adjoining listric fault surfaces F1 and F2 shown in Fig. 3. We can describe the fault surfaces by:

$$\text{F1} \rightarrow z_1^{\text{T}} = -z_0(1 - e^{-d_1/\lambda_1}) \tag{A1}$$

$$\text{F2} \rightarrow z_2^{\text{T}} = -z_0(1 - e^{-d_2/\lambda_2}), \tag{A2}$$

where z_i^{T} is the depth of a point on the fault surface, z_0 is the depth to detachment, λ_i is a constant that characterizes the curvature of the fault plane, and d_i is the horizontal distance from the surface trace of the fault to the horizontal projection of any point (x, y) on the fault(s) surface in a direction perpendicular to the fault strike. For α_1, α_2 and β as defined on Fig. 3:

$$d_1 = \sqrt{x^2 + y^2}\sin(\beta - \alpha_1) \tag{A3}$$

$$d_2 = \sqrt{x^2 + y^2}\sin(\alpha_2 - \beta). \tag{A4}$$

By the identity expansion of the sine of the difference of two angles and by substitution of right triangle identities into equations (A3) and (A4) they become:

$$d_1 = y\cos\alpha_1 - x\sin\alpha_1 \tag{A5}$$

$$d_2 = x\sin\alpha_2 - y\cos\alpha_2. \tag{A6}$$

It is apparent from equations (A1) and (A2) that the fault surfaces intersect at:

$$d_1/\lambda_1 = d_2/\lambda_2. \tag{A7}$$

Substituting (A5) and (A6) into (A7) yields:

$$\lambda_2(y\cos\alpha_1 - x\sin\alpha_1) = \lambda_1(x\sin\alpha_2 - y\cos\alpha_2).$$

Rearranging in terms of x and y gives the relationship:

$$x(\lambda_1\sin\alpha_2 + \lambda_2\sin\alpha_1) = y(\lambda_1\cos\alpha_2 + \lambda_2\cos\alpha_1). \tag{1}$$

The direction of extension is equivalent to the maximum horizontal displacement vector or the direction of the intersection of the two fault planes and thus can be given as:

$$\varepsilon_{\text{h}} = \beta = \arctan\left(\frac{\lambda_1\sin\alpha_2 + \lambda_2\sin\alpha_1}{\lambda_1\cos\alpha_2 + \lambda_2\cos\alpha_1}\right).$$

APPENDIX 2

Derivation of the dip of the hangingwall surface in a three-dimensional listric fault system when the hangingwall is deformed by vertical shear

A random point, (x_a, y_a), on the surface ($z^S = 0$) of the undeformed hangingwall is translated in the direction of the tectonic track and is located at (x_b, y_b) in the deformed state. Translation along the track or in the direction of ε_h as derived in Appendix 1 ensures that a point originally overlying one fault will remain above the same fault after deformation. If the block undergoes vertical shear, a surface point's new depth, z^S, is given by:

$$z^S = z_b^T - z_a^T, \tag{A8}$$

where z_i^T is the depth to the fault plane before and after translation. These depths are given by:

$$z_a^T = -z_o(1 - e^{-d_a/\lambda_1}) \quad \text{and} \quad z_b^T = -z_o(1 - e^{-d_b/\lambda_1}).$$

Substituting the pre- and post-deformation relationships above into (A8) gives the new depth as:

$$z^S = -z_o(e^{-d_a/\lambda_1} - e^{-d_b/\lambda_1}). \tag{A9}$$

The translation motion, δu, is in the direction of β so that:

$$x_a = x_b - \delta u \cos\beta \quad \text{and} \quad y_a = y_b - \delta u \sin\beta. \tag{A10}$$

Since d_i in (A9) is given by the relationship in (A3) as:

$$d_a = y_a \cos\alpha_1 - x_a \sin\alpha_1$$

and

$$d_b = y_b \cos\alpha_1 - x_b \sin a_1$$

we can solve for d_a in terms of β and d_b:

$$\begin{aligned} d_a &= (y_b - \delta u \sin\beta)\cos\alpha_1 - (x_b - \delta u \cos\beta)\sin\alpha_1 \\ &= y_b \cos\alpha_1 - x_b \sin\alpha_1 + \delta u \cos\beta \sin\alpha_1 - \delta u \sin\beta \cos\alpha_1 \\ &= d_b + \delta u(\cos\beta \sin\alpha_1 - \sin\beta \cos\alpha_1) \\ &= d_b + \delta u \sin(\alpha_1 - \beta). \end{aligned} \tag{A11}$$

Substituting (A11) into (A9) yields:

$$\begin{aligned} z^S &= -z_o(e^{-d_b/\lambda_1} e^{-\delta u \sin(\alpha_1 - \beta)/\lambda_1} - e^{-d_b/\lambda_1}) \\ &= -z_o e^{-d_b/\lambda_1}(e^{-\delta u \sin(\alpha_1 - \beta)/\lambda_1} - 1). \end{aligned} \tag{A12}$$

To simplify our calculation of the dip of the hangingwall surface we define z_o^D as:

$$z_o^D = z_o(e^{\delta u \sin(\beta - \alpha_1)/\lambda_1} - 1)$$

a quantity that is independent of d_b. Substituting it into (A12) the surface of the block is given by:

$$z_1^S = -z_o^D e^{-d_b/\lambda_1} \tag{A13}$$

in the region over F1. The same result may be derived for a point in the region over F2:

$$z_2^S = -z_o^D e^{-d_b/\lambda_2}.$$

Note that z_o^D is the same in both regions as:

$$\frac{\sin(\beta - \alpha_1)}{\lambda_1} = \frac{\sin(\alpha_2 - \beta)}{\lambda_2}.$$

The dip of the hangingwall surface, $\tan\delta$, in a random direction s which makes an angle θ with the x-axis (Fig. 3) is given by the derivative of the surface function (A13) with respect to s:

$$\begin{aligned} \tan\delta &= \frac{dz^S}{ds} \\ &= \frac{\partial z^S}{\partial x}\frac{\partial x}{\partial s} + \frac{\partial z^S}{\partial y}\frac{\partial y}{\partial s} \\ &= \frac{\partial z^S}{\partial x}\cos\theta + \frac{\partial z^S}{\partial y}\sin\theta. \end{aligned}$$

The dip of the hangingwall surface over F1 can then be written as:

$$\begin{aligned} \tan\delta &= \frac{-z_o^D}{\lambda_1}\left(\frac{\partial d_1}{\partial x}\cos\theta + \frac{\partial d_1}{\partial y}\sin\theta\right)e^{-d_1/\lambda_1} \\ &= \frac{-z_o^D}{\lambda_1}(-\sin\alpha_1\cos\theta + \cos\alpha_1\sin\theta)\,e^{-d_1/\lambda_1} \\ &= \frac{-z_o}{\lambda_1}\sin(\theta - \alpha_1)\,e^{-d_1/\lambda_1}. \end{aligned} \tag{A14}$$

Since $(-z_o^D/\lambda_1)$ and e^{-d_1/λ_1} are constants, the maximum dip direction of the hangingwall surface is when $\theta = \alpha_1 + (\pi/2)$ or perpendicular to F1. By a similar derivation the dip of the hangingwall over F2 is given by:

$$\tan\delta = \frac{-z_o^D}{\lambda_2}\sin(\alpha_2 - \theta)\,e^{-d_2/\lambda_2}$$

again indicating a maximum dip direction perpendicular to the fault (F2) when $\theta = (\alpha/2)$. Dip directions into F1 and F2 will create a ridge on the hangingwall surface over the tectonic track in the direction of ε_h or β in a three-dimensional extensional listric fault system that undergoes vertical shear.